(Preprint) AAS 25-371

STATION-KEEPING FOR EARTH-MOON PERIODIC ORBIT WITH SOLAR SAIL BASED ON THE ORBIT-ATTITUDE COUPLED MODEL

Yuta Hayashi[*], Naoki Hiraiwa[*], Mai Bando[†], and Shinji Hokamoto[†]

Solar sails are propulsion mechanisms that use solar radiation pressure to propel a spacecraft. Although the propulsive force is small, which is very useful for long-term exploration. This study discusses the stable orbit and attitude controllability of a spacecraft orbiting in a periodic orbit near the Moon with a solar sail. We also discuss the effect of the propulsive force, which varies by changing the orientation of the sail, on the orbit of the spacecraft and station keeping based on Floquet modes. In numerical simulations, both motions are controlled by considering the effect of the attitude motion on the orbital motion, and the robustness of the orbit and attitude control as a coupled orbit-attitude model is confirmed. Finally, this study demonstrates that solar sails are effective in maintaining long-term stability of periodic orbits and highlights their practical potential for future deep space exploration.

INTRODUCTION

Rapid progress in deep space exploration has attracted scientific and technological attention to the use of Lyapunov orbits (2D periodic orbits) and halo orbits (3D periodic orbits)[1,2] near the Earth-Moon L_2 point. The analysis of spacecraft motion using these periodic orbits has been extensively discussed mainly as the Circularly Restricted Three-Body Problem (CRTBP).[3–7] These orbits provide stable platforms for wide-area observation, long-duration exploration missions, and enhanced communication infrastructure. However, while these periodic orbits are dynamically advantageous, their long-duration stability is highly susceptible to perturbations, numerical errors, and uncertainties, so precise orbit control techniques are required to ensure mission success.[8–10] Furthermore, conventional thruster-based systems constrained by finite fuel resources pose a significant challenge to keeping spacecraft in nominal orbit for long-durations. To address this challenge, this study applies solar sail technology to orbit control around the Earth-Moon L_2 point. Unlike traditional propulsion systems reliant on consumable fuel, solar sails utilize Solar Radiation Pressure (SRP) to generate continuous propulsion, enabling sustainable station-keeping. The force due to the solar sail is parameterized mainly by its direction (defined by two angles α and δ).[11–13]

In this study, Floquet modes are employed to evaluate the stability of the orbit and analyze the growth and attenuation of perturbations to achieve orbit control. Additionally, the necessary sail attitude adjustments for orbit control are implemented using quaternion feedback. For station-keeping based on the Floquet modes, ideas from References 4 and 5 concerning station-keeping around equilibrium points are adopted to address station-keeping for solar sails near

[*]Doctoral student, Department of Aeronautics and Astronautics, Kyushu University, 819-0395.
[†]Professor, Department of Aeronautics and Astronautics, Kyushu University, 819-0395.

halo orbits. First, it is essential to understand the phase space behavior around the nominal orbit and how changes in sail attitude affect the orbital motion. The orbit-attitude coupled model[14,15] analysis provides critical insights into the design of orbit and attitude control. Although fully coupled model control has not been implemented, considering the coupling effect of the two motions contributes to improved control performance. The primary objective of this study is to independently control the dynamics of orbit and attitude while appropriately analyzing their coupling effects to ensure overall system stability and efficiency.

A station-keeping strategy is necessary to keep near the halo orbit over extended periods. This study discusses the controllability of these orbits and proposes methods for deriving efficient station-keeping strategies using solar sails. The proposed method calculates control inputs for orbit stabilization using SRP based on the Floquet modes. Subsequently, the derived attitude control history is used to control the spacecraft's attitude and achieve the desired attitude. Quaternion feedback is employed to realize robust and efficient attitude correction, providing a framework for independently executing orbit and attitude control.

To verify the proposed method, numerical simulations of a spacecraft orbiting in a halo orbit near the Earth-Moon L_2 point are performed. Through accurate orbit control and attitude stabilization, this study addresses critical issues in multi-body dynamics, provides a foundation for sustainable deep space exploration, and enhances the feasibility of long-term exploration missions.

DYNAMICAL MODEL

Consider the motion of a solar sail spacecraft(sometimes abbreviated simply as sail) moving under the gravitational force from P_1 (Earth) and P_2 (Moon), the masses of the Earth and the Moon are denoted as m_1 and m_2, respectively. r_1, r_2 are the distances of a spacecraft from the Earth and the Moon. In Fig. 1), let (X, Y, Z) be the inertial coordinate system whose origin is the barycenter of the system, and (x, y, z) be the rotating coordinate system with the barycenter of the system as the origin and the x-axis is defined by the direction vector from the primary to the secondary body, and (b_1, b_2, b_3) be the body-fixed coordinate system whose origin is at the center of mass of a spacecraft. Within this coordinate system, a spacecraft is considered to be affected by the gravitational forces of two celestial bodies, m_1 (Earth) and m_2 (Moon). Assuming these two celestial bodies undergo circular motion around their common barycenter, the motion of a spacecraft with a mass m that is significantly smaller than m_1 and m_2 is analyzed. This framework is referred to as the CRTBP. Figure 2 shows the Earth-Moon rotational coordinate system taking into account the solar sail. The model assumes that the Sun is moving in a circular motion on the xy plane of the Earth-Moon rotational coordinate system. This assumption simplifies the analysis of the solar sails. The spacecraft allows station-keeping and orbital maneuvers without consuming fuel by utilizing the continuous thrust generated by the SRP acceleration. This acceleration is affected by the sail attitude relative to the direction of incoming sunlight. This attitude is parameterized by two angles α and δ. The equations of motion described below are nondimensionalized so that the distance between the Earth and the Moon (384,400 km) and the inverse of the angular velocity are normalized.

Orbital Dynamics

The dimensionless Earth-Moon mass parameter μ is expressed as $\mu = m_2/(m_1 + m_2)$ with masses m_1 and m_2 for the Earth and Moon, respectively. The equations of motion of the CRTBP in

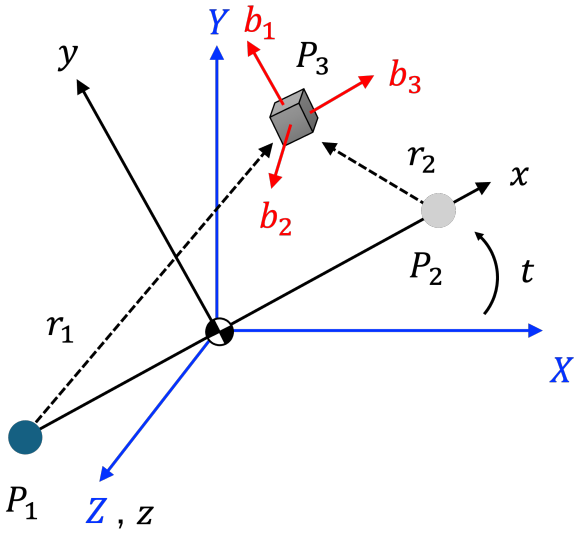

Figure 1: Schematic of CRTBP

a rotating coordinate system with x, y, z as the origin are given by

$$\begin{aligned}
\ddot{x} &= x + 2\dot{y} - \frac{(1-\mu)(x+\mu)}{r_1^3} - \frac{\mu(x-1+\mu)}{r_2^3} \\
\ddot{y} &= y - 2\dot{x} - \frac{(1-\mu)y}{r_1^3} - \frac{\mu y}{r_2^3} \\
\ddot{z} &= -\frac{(1-\mu)z}{r_1^3} - \frac{\mu z}{r_2^3}
\end{aligned} \tag{1}$$

In addition, there exists a conserved quantity called the Jacobi constant as follows:

$$C = x^2 + y^2 + \frac{2(1-\mu)}{r_1} + \frac{2\mu}{r_2} - (\dot{x}^2 + \dot{y}^2 + \dot{z}^2) \tag{2}$$

The equilibrium point of Eq. (1) is called the Lagrangian point where gravity and centrifugal force balance. Figure 3 shows the halo orbits near the Earth-Moon L_2 point. The color bar shows the Jacobi constant for each orbit, and the orbits are colored based on the Jacobi constant. Furthermore, it is known that there exists a family of planar periodic orbits called Lyapunov orbits and a family of spatial periodic orbits called halo orbits around the collinear libration points. In addition, as shown in Fig. 2, the dynamical equations of the solar sail due to SRP acceleration is expressed as follows:

$$\begin{aligned}
\ddot{x} &= x + 2\dot{y} - \frac{(1-\mu)(x+\mu)}{r_1^3} - \frac{\mu(x-1+\mu)}{r_2^3} + a_x \\
\ddot{y} &= y - 2\dot{x} - \frac{(1-\mu)y}{r_1^3} - \frac{\mu y}{r_2^3} + a_y \\
\ddot{z} &= -\frac{(1-\mu)z}{r_1^3} - \frac{\mu z}{r_2^3} + a_z
\end{aligned} \tag{3}$$

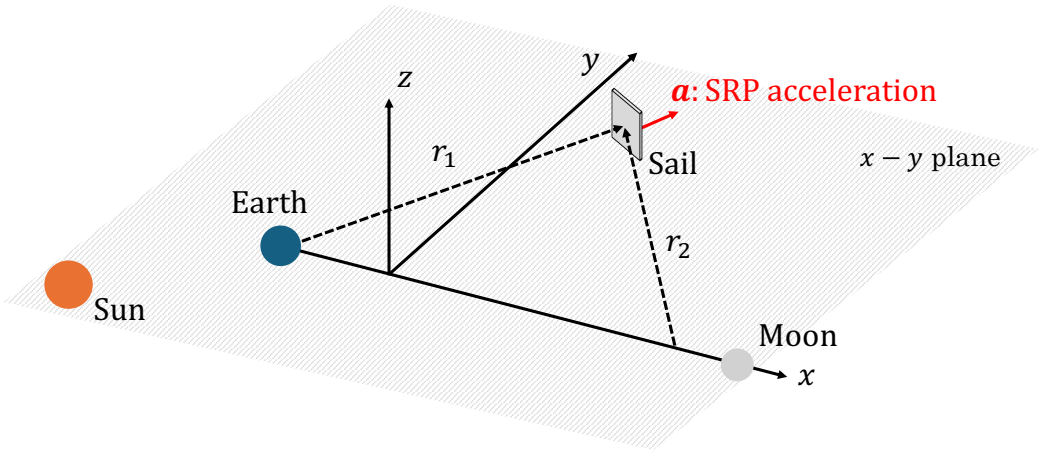

Figure 2: Schematic of Solar Sail Earth-Moon CRTBP

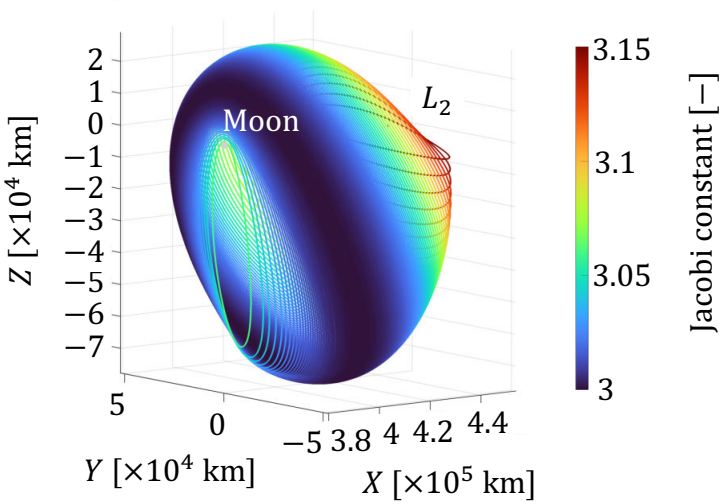

Figure 3: L_2 Halo Orbits

Solar sail steering law

The term a in Eq. (3) represents the SRP acceleration. To define this acceleration, the sail is assumed to be a perfect reflective mirror without wrinkles or other optical defects. The sail gains propulsion by mirror-reflecting photons from sunlight, generating an acceleration in the direction of the unit vector $\vec{\boldsymbol{n}}$, which is normal to the sail's surface. Based on this assumption, the SRP acceleration acting on a flat reflective surface is given as follows:[16,17]

$$\begin{aligned}\boldsymbol{a} &= [a_x, a_y, a_z]^T \\ &= -\frac{S_0}{c}\frac{A}{m}\left(\frac{1}{D}\right)^2 \left[|\vec{\boldsymbol{s}}\cdot\vec{\boldsymbol{n}}|(C_a + C_d)\vec{\boldsymbol{s}} + (\vec{\boldsymbol{s}}\cdot\vec{\boldsymbol{n}})(B_f C_d + C_a\kappa + 2C_s|\vec{\boldsymbol{s}}\cdot\vec{\boldsymbol{n}}|)\vec{\boldsymbol{n}}\right] \end{aligned} \tag{4}$$

where A, m, S_0, c and D represent the area of the reflective surface, solar sail spacecraft mass, solar constant ($1366[\mathrm{W/m^2}]$), velocity of light ($3.0 \times 10^8[\mathrm{m/s}]$), and distance between the Sun and

solar sail in astronomical unit (au), respectively. C_a, C_s, and C_d are the coefficient of absorption, the coefficient of specular reflection, and the coefficient of diffusive reflection, respectively. B_f and κ are the Lambertian coefficient $(2/3)$ and the thermal emissivity (0). The SRP acceleration of a solar sail primarily depends on the direction vector of sunlight $\vec{\boldsymbol{s}}$ and the normal vector of the sail $\vec{\boldsymbol{n}}$. Fist the direction vector of sunlight $\vec{\boldsymbol{s}}$, the vector is defined as $\vec{\boldsymbol{s}} = [-\cos(\Omega_s t), \sin(\Omega_s t), 0]^T$. Ω is the apparent dimensionless angular velocity of the Sun in the Earth-Moon rotational coordinate system, which is $\Omega = 0.9252$.

Here, α represents the solar incidence angle within the xy plane in the spacecraft-fixed coordinate system, as shown in Fig. 4a, which indicates the direction in the xy plane.[12] For the other, δ represents the out-of-plane angle in the body-fixed coordinate system as shown in Fig. 4b, which indicates how much the direction of sunlight deviates from the xz plane.

$$\vec{\boldsymbol{n}} = \begin{bmatrix} -\sin(\Omega_s t)\sin\alpha\cos\delta + \cos(\Omega_s t)\cos\alpha\cos\delta \\ -\sin(\Omega_s t)\cos\alpha\cos\delta - \cos(\Omega_s t)\sin\alpha\cos\delta \\ -\sin\delta \end{bmatrix} \tag{5}$$

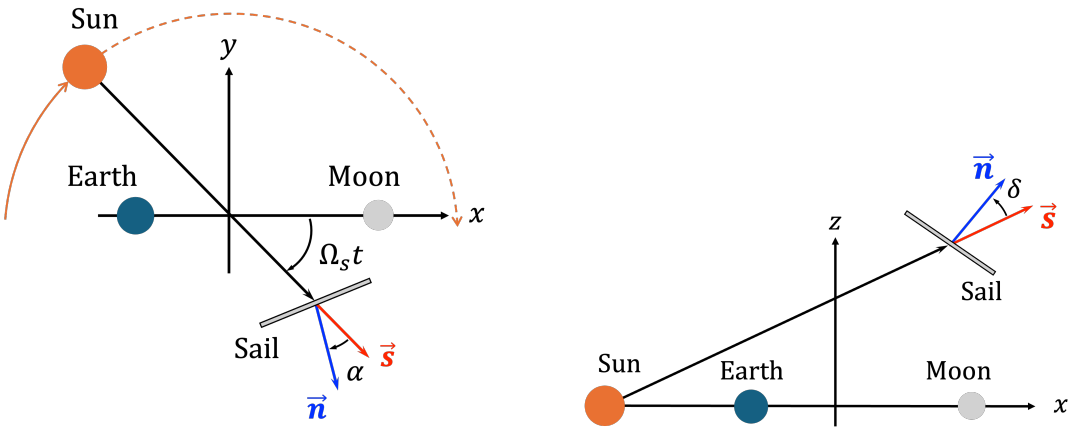

(a) In-Plane Angle α (b) Out-of-Plane Angle δ

Figure 4: Schematic of Sail Angle

Attitude Dynamics

The Euler's equation of motion for the sail is described by the rotational dynamics as follows:

$$J\dot{\boldsymbol{\omega}} + \omega^{\times} J\boldsymbol{\omega} = \boldsymbol{T}_{Ctrl} + \boldsymbol{T}_{\mathrm{GG}} + \boldsymbol{T}_{\mathrm{SRP}} \tag{6}$$

where J is the inertia moment of a solar sail spacecraft and $\boldsymbol{\omega} = [\omega_1, \omega_2, \omega_3]^T$ is the angular velocity vector. $\boldsymbol{T}_{Ctrl} = [T_{Ctrl,1}, T_{Ctrl,2}, T_{Ctrl,3}]^T$ is the control torque derived from the attitude control system of a spacecraft. $\boldsymbol{T}_{\mathrm{GG}}$ is the disturbance torque due to the Gravity Gradient (GG) from the Earth and Moon. $\boldsymbol{T}_{\mathrm{SRP}}$ is the disturbance torque due to the SRP from the Sun. $^{\times}$ denotes the cross-product, defined by the following skew-symmetric matrix.

$$v^{\times} = \begin{bmatrix} 0 & -v_3 & v_2 \\ v_3 & 0 & -v_1 \\ -v_2 & v_1 & 0 \end{bmatrix} \tag{7}$$

GG torque $\boldsymbol{T}_{\mathrm{GG}}$ is described as follows:

$$\boldsymbol{T}_{\mathrm{GG}} = \frac{3(1-\mu)}{r_1^5}(-g^{\times} J\boldsymbol{g}) + \frac{3\mu}{r_2^5}(-h^{\times} J\boldsymbol{h}) \tag{8}$$

where $\boldsymbol{g}$ and $\boldsymbol{h}$ are written using the Direction Cosine Matrix (DCM) and spacecraft's position vector as follows:

$$\boldsymbol{g} = \begin{bmatrix} g_1 \\ g_2 \\ g_3 \end{bmatrix} = [A_{b/i}][A_{i/r}]\boldsymbol{r_1}, \qquad \boldsymbol{h} = \begin{bmatrix} h_1 \\ h_2 \\ h_3 \end{bmatrix} = [A_{b/i}][A_{i/r}]\boldsymbol{r_2} \tag{9}$$

$[A_{i/r}]$ is the DCM for converting the rotation coordinate system to the inertial coordinate system and $[A_{b/i}]$ is the DCM for converting the inertial coordinate system to the body-fixed coordinate system of a spacecraft are given as follows:

$$A_{i/r} = \begin{bmatrix} \cos(t) & \sin(t) & 0 \\ -\sin(t) & \cos(t) & 0 \\ 0 & 0 & 1 \end{bmatrix} \tag{10}$$

$$A_{b/i} = \begin{bmatrix} q_1^2 - q_2^2 - q_3^2 + q_4^2 & 2(q_1q_2 + q_3q_4) & 2(q_1q_3 - q_2q_4) \\ 2(q_1q_2 - q_3q_4) & -q_1^2 + q_2^2 - q_3^2 + q_4^2 & 2(q_2q_3 + q_1q_4) \\ 2(q_1q_3 + q_2q_4) & 2(q_2q_3 - q_1q_4) & -q_1^2 - q_2^2 + q_3^2 + q_4^2 \end{bmatrix} \tag{11}$$

For the SRP torque, similar to GG torque, a DCM is introduced to convert it from the rotational coordinate system to the body-fixed coordinate system. The SRP torque $\boldsymbol{T}_{\mathrm{SRP}}$ in the body-fixed coordinate system is defined as the product of the SRP acceleration on the solar sail and the sail position vector.

$$\boldsymbol{T}_{\mathrm{SRP}} = [A_{b/i}][A_{i/r}]\,(\vec{\boldsymbol{r}} \times \boldsymbol{a}) \tag{12}$$

where $\vec{\boldsymbol{r}}$ is the relative position vector from the center of gravity of each spacecraft segment.

Attitude Kinematics

The attitude kinematics is described following equation for the rotation axis relative to either an inertial coordinate system $\boldsymbol{k} = [k_1, k_2, k_3]^T$ and the rotation angle θ and using quaternion. The attitude quaternion is defined as follows:

$$\begin{bmatrix} \boldsymbol{q} \\ q_4 \end{bmatrix} = \begin{bmatrix} \boldsymbol{k} \sin\frac{\theta}{2} \\ \cos\frac{\theta}{2} \end{bmatrix} \tag{13}$$

where $\boldsymbol{q} = [q_1, q_2, q_3]^T$ and the constraints must be satisfied: $\boldsymbol{q}^2 + q_4^2 = 1$.
The quaternion kinematic equations in body-fixed coordinate system are given as follows:

$$\begin{bmatrix} \dot{\boldsymbol{q}} \\ \dot{q}_4 \end{bmatrix} = \frac{1}{2}\begin{bmatrix} q_4 I_3 + q^{\times} \\ -\boldsymbol{q}^T \end{bmatrix}\boldsymbol{\omega} \tag{14}$$

where I_3 is a unit matrix of 3×3.

Attitude Error Dynamics

In the convergence problem, define the target angular velocity and quaternion of a spacecraft as $\boldsymbol{\omega}_d \in \mathbb{R}^3$ and $[\boldsymbol{q}_d, q_{4d}]^T = [q_{1d}, q_{2d}, q_{3d}, q_{4d}]^T$. Also, error dynamics and kinematics are described as follows:

$$J\delta\dot{\boldsymbol{\omega}} = -\omega^{\times} J\boldsymbol{\omega} + J\{\delta\omega^{\times} R[\delta\bar{q}]\boldsymbol{\omega}_d - R[\delta\bar{q}]\dot{\boldsymbol{\omega}}_d\} + \boldsymbol{T}_{Ctrl} + \boldsymbol{T}_{\mathrm{GG}} + \boldsymbol{T}_{\mathrm{SRP}} \tag{15}$$

$$\begin{bmatrix} \delta\dot{\boldsymbol{q}} \\ \delta\dot{q}_4 \end{bmatrix} = \frac{1}{2} \begin{bmatrix} \delta q_4 I_3 + q^{\times} \\ -\delta\boldsymbol{q}^T \end{bmatrix} \delta\boldsymbol{\omega} \tag{16}$$

where $\delta\boldsymbol{\omega}$ denotes the error angular velocity derived by the following equation.

$$\delta\boldsymbol{\omega} = \boldsymbol{\omega} - R[\delta\bar{q}]\boldsymbol{\omega}_d \tag{17}$$

R is the rotation matrix, $\delta\bar{q}$ is the error quaternion. The error quaternion $\delta\bar{q} = [\delta\boldsymbol{q}^T, \delta q_4]^T$ denotes the error from the desired quaternion.

STATION-KEEPING WITH SOLAR SAIL

Linearized dynamics around halo orbit

The behavior around periodic orbits is generally analyzed by first-order variational equations. The flow ϕ associated with the equations of motion for a given small perturbation h is described as follows:[18]

$$\phi_\tau(x_0 + h) = \phi_\tau(x_0) + D\phi_\tau(x_0) \cdot h + O(|h|^2) \tag{18}$$

where the flow $\phi_\tau(x_0)$ represents the transition of the initial state $x_0 \in \mathbb{R}^6$ from time t_0 to τ. $D\phi_\tau(x_0)$ is the first-order variational of the flow $\phi_\tau(x_0)$. $D\phi_\tau(x_0)\cdot h$ is defined good approximation of the flow $\phi_\tau(x_0 + h)$. From this, the linearization of dynamics around a periodic orbit of period time T is based on the eigenvalues and eigenvectors of the monodromy matrix associated with the natural periodic orbit. The eigenvalues of the monodromy matrix are represented by six eigenvalues $\lambda_{1,\ldots,6}$ (in pairs of three $\{(\lambda_1, \lambda_2), (\lambda_3, \lambda_4), (\lambda_5, \lambda_6)\}$) that have the following geometric meaning and characterize the stability and periodicity of the halo orbit.

The first pair (λ_1, λ_2)

The eigenvalues satisfy $(\lambda_1 \cdot \lambda_2 = 1)$ and are associated with the hyperbolic nature of the orbit. The value λ_1, which has the largest absolute value, is related to the eigenvector $e_1(0)$, indicating the most expanding direction. After one period, the distance from the nominal orbit in this direction is amplified by a factor of λ_1. Under the variational flow, the image of this vector is given using $D\phi_\tau$ as follows:

$$e_1(\tau) = D\phi_\tau e_1(0) \tag{19}$$

At each point on the orbit, the vector $e_1(\tau)$, together with the vector tangent to the orbit, spans a plane that is tangent to the local unstable manifold. Similarly, λ_2 and its associated eigenvector $e_2(0)$ are related to the stable manifold, satisfying the relation as follows:

$$e_2(\tau) = D\phi_\tau e_2(0) \tag{20}$$

The second pair (λ_3, λ_4)

These are complex conjugate eigenvalues with modulus 1. The other two eigenvalues are equal to 1, and these indicate central motion around a periodic orbit. The monodromy matrix, restricted to the plane spanned by the real $e_3(0)$ and imaginary $e_4(0)$ parts of the eigenvectors associated to $\lambda_3, \lambda 4$, which described as a rotation of angle: $\Gamma = \arctan(\mathrm{Im}(\lambda_3)/\mathrm{Re}(\lambda_3))$, the argument of λ_3.

The third pair (λ_5, λ_6)

These eigenvalues satisfy $(\lambda_5 = \lambda_6 = 1)$ and are associated with neutral directions. This vector is the tangent vector to the orbit, denoted as $e_5(0)$. The other eigenvalue is related to variations in the period or other variables characterizing the family of periodic orbits. The corresponding eigenvector is chosen orthogonal to $e_5(0)$ in the 2D subspace associated with the eigenvalue and provides the tangent direction to the family of halo orbits. The monodromy matrix restricted to this plane takes the form:

$$\begin{pmatrix} 1 & \varepsilon \\ 0 & 1 \end{pmatrix} \tag{21}$$

The variational flow of each component is defined as follows, which determines the change in phase space characteristics in a small neighborhood of the periodic orbit.

$$e_i(\tau) = D\phi_\tau \cdot e_i(0), \quad i = 1, \ldots, 6 \tag{22}$$

From the above, the value ε is due to variations in the period as the orbit changes within the family. Finally, the monodromy matrix associated with a halo orbit is described as follows:

$$J = \begin{pmatrix} \lambda_1 & & & & 0 & \\ & \lambda_2 & & & & \\ & & \cos\Gamma & -\sin\Gamma & & \\ & & \sin\Gamma & \cos\Gamma & & \\ & 0 & & & 1 & \varepsilon \\ & & & & 0 & 1 \end{pmatrix} \tag{23}$$

Floquet modes in the reference system

Based on the ideas of station-keeping around the halo orbit,[19] Reference 13 using conventional propulsion in the Sun-Earth dynamics and the station-keeping with solar sails around the equilibrium point,[18,20] this study is focused on station-keeping around the L_2 periodic orbit in the Earth-Moon dynamics. In this method, it is very important to track the state of the spacecraft with respect to stable and unstable manifolds at all times, and the objective is to derive the optimal sail attitude change to correct to a nominal orbit at the time of escape from the orbit. The Floquet modes are used to obtain a suitable reference system on the halo orbit. The main idea of the method is to allow the orbit to track the natural dynamics of the system and to allow the orbit to escape along the unstable manifold. If the solar sail diverges significantly from the nominal orbit, an appropriate new solar sail attitude is selected and adjusted so that the orbit is close to the stable manifold and the error in the orbit central motion is minimized. To find this new solar sail attitude, we also use the linear map described as follows.

$$\mathcal{F}(\Delta t, \Delta\alpha, \Delta\delta) = \phi_{\Delta t}(t_0, x_0, \alpha_0, \delta_0) + \frac{\partial \phi_{\Delta t}}{\partial \alpha}(t_0, x_0, \alpha_0, \delta_0) \cdot \Delta\alpha + \frac{\partial \phi_{\Delta t}}{\partial \delta}(t_0, x_0, \alpha_0, \delta_0) \cdot \Delta\delta \tag{24}$$

where $\phi_{\Delta t}(t_0, x_0, \alpha_0, \delta_0)$ is the first-order approximation of the flow at time $t_1 = t_0 + \Delta t$, starting from $t = t_0$. For $\mathcal{F}(\Delta t, \Delta\alpha, \Delta\delta)$, note that for a given initial state x_0, the change $\Delta\alpha, \Delta\delta$ to the sail

attitude at time $t = t_0$ provides a first-order approximation of the orbit states at time $t = t_0 + \Delta t$. Using this characteristic, it is possible to find the appropriate change $\Delta\alpha, \Delta\delta$ to bring the orbit closer to the nominal orbit after a given time Δt. The first-order variational flow gives information on how small variations in the initial states affect the little further state.

From here on, we replace the function $e_i(\tau) = D\phi_\tau \cdot e_i(0)$ presented above to characterize the behavior of periodic orbits and introduce a simpler six T-periodic functions, the Floquet modes $\bar{e}_i(\tau), \quad i = 1, \ldots 6$. The advantage of Floquet modes is that they can be extended as a Fourier series and easily conserved by their Fourier coefficients. Furthermore, the Floquet modes provide a highly useful reference frame for continuously tracking the relative position of the spacecraft's current state with respect to the local unstable and stable invariant manifolds of the nominal orbit.

Following Reference 19, we define the first and second Floquet modes, considering that the escape along the unstable manifold and the approach to the halo orbit along the stable manifold occur at exponential rates.

$$\bar{e}_1(\tau) = e_1(\tau) \exp\left(-\frac{\tau}{T} \ln \lambda_1\right) \tag{25}$$

$$\bar{e}_2(\tau) = e_2(\tau) \exp\left(-\frac{\tau}{T} \ln \lambda_2\right) \tag{26}$$

The third and fourth modes are calculated by considering that the monodromy matrix represents a rotation by an angle Γ within the plane spanned by the real and imaginary parts of the eigenvectors associated with λ_3 and λ_4.

$$\bar{e}_3(\tau) = \cos\left(-\frac{\Gamma\tau}{T}\right) e_3(\tau) - \sin\left(-\frac{\Gamma\tau}{T}\right) e_4(\tau) \tag{27}$$

$$\bar{e}_4(\tau) = \sin\left(-\frac{\Gamma\tau}{T}\right) e_3(\tau) + \cos\left(-\frac{\Gamma\tau}{T}\right) e_4(\tau) \tag{28}$$

Finally, the fifth mode is the vector tangent to the halo orbit, while the sixth mode is chosen to be orthogonal to $\bar{e}_5(t)$ within the plane spanned by $e_5(t)$ and $e_6(t)$.

$$\bar{e}_5(\tau) = e_5(\tau) \tag{29}$$

$$\bar{e}_6(\tau) = e_6(\tau) - \varepsilon(\tau)\bar{e}_5(\tau) \tag{30}$$

The dynamics around a halo orbit are equivalent to those obtained when using the functions $e_i(t)$ as the reference system. Specifically, along the planes spanned by $\bar{e}_1(t)$ and $\bar{e}_2(t)$, the trajectory escapes in the unstable direction $\bar{e}_1(t)$. On the planes spanned by $\bar{e}_3(t)$ and $\bar{e}_4(t)$, the trajectory rotates around the periodic orbit. Lastly, on the planes spanned by $\bar{e}_5(t)$ and $\bar{e}_6(t)$, the dynamics are neutral. Note that the station-keeping method described here determines the change in solar sail attitude based on the linearized dynamics of the system.

Orbit control method

The solar sail is controlled to remain close to the nominal orbit $N_0(t)$, starting with fixed sail attitude $\alpha = 0$ and $\delta = \delta_0$. The orbit error $\bar{e}_i(t)$ is defined based on the Floquet modes, which form the reference frame. Using this reference frame, orbit tracking is performed to determine when and how the sail attitude should be adjusted.

To fix the notation, let φ denote the position and velocity of the solar sail at time t_0. In this reference frame, it can be expressed as follows:

$$\varphi(t_0) = N_0(t_0) + \sum_{i=1}^{6} s_i(t_0)\bar{e}_i(t_0) \tag{31}$$

To ensure mission success, three parameters ($\varepsilon_{\max}$, $dt_{\min}$, and $dt_{\max}$) need to be defined for each mission. These parameters depend on the mission requirements and the dynamics of the system around the nominal orbit $N_0(t)$. $\varepsilon_{\max}$ represents the maximum allowable error distance in the stable direction and is used to determine when to adjust the sail attitude.

When the sail's trajectory approaches the nominal orbit $(N_0(t))$, the sail attitude, $\alpha = 0, \delta = \delta_0$, is set. Due to the presence of a saddle structure, the trajectory tends to escape in an unstable direction. When $|s_1(t_1)| > \varepsilon_{\max}$ the sail is escaping, it becomes necessary to adjust the sail attitude. Referring to Eq. (24), the new sail angles α_1 and δ_1, along with the time dt_1 within the range $[dt_{\min}, dt_{\max}]$, are determined. At the current time $t = t_1 + dt_1$, the sail attitude is changed, and the sail trajectory is adjusted to approach the nominal orbit $N_0(t_1 + dt_1)$. Finally, at $t_1 + dt_1$, the sail attitude is restored. This process is repeated throughout the duration of the mission to ensure orbit correction and stability.

Search method for α_1, δ_1 and dt_1

Assume that at time $t = t_1$, $|s_1(t_1)| > \varepsilon_{\max}$, and a new sail attitude needs to be chosen. Recall that $\mathcal{F}$ is a linear mapping and that small changes in the sail attitudes $\Delta\alpha$ and $\Delta\delta$ at $t = t_1$ affect the sail's trajectory at time $t = t_1 + \Delta t$. Our main objective is to determine $\Delta\alpha, \Delta\delta$, and dt_1 such that the flow at time $t = t_1 + dt_1$ is close to the stable manifold. Specifically, this means ensuring that $s_1(t_1 + dt_1)$ is small while preventing the central projections $(s_3(t_1 + dt_1), s_4(t_1 + dt_1))$ and $(s_5(t_1 + dt_1), s_6(t_1 + dt_1))$ from becoming excessively large.

The process can proceed as follows:

1. Here, consider the time interval $[t_1 + dt_{\min}, t_1 + dt_{\max}]$ with $i = 0, \ldots, n$. Define $\tilde{t}_i = t_1 + dt_{\min} + i \cdot dt$, where $dt = (dt_{\max} - dt_{\min})/n$. For each $\tilde{t}_i$, calculate the variational map $\mathcal{F}$ given by Eq. (24).

2. For each $\tilde{t}_i$, find $\Delta\alpha_i$ and $\Delta\delta_i$ such that $s_1(\tilde{t}_i) = s_5(\tilde{t}_i) = s_6(\tilde{t}_i) = 0$. Note that this involves solving a system of equations with two unknown variables and three equations, which will be addressed using the least-squares method. Finally, a set of $\{\tilde{t}_i, \Delta\alpha_i, \Delta\delta_i\}_{i=1,\ldots,n}$ is obtained, ensuring that $(s_1(t_i), s_5(t_i), s_6(t_i))$ remains small.

3. From the set $\{\tilde{t}_i, \Delta\alpha_i, \Delta\delta_i\}_{i=1,\ldots,n}$ obtained in Step 2, choose $\tilde{t}_j, \Delta\alpha_j, \Delta\delta_j$ such that $(s_3(t_j), s_4(t_j))$ are minimized.

The parameters for bringing the sail back to the nominal orbit obtained by using this method are as follows:

$$\alpha_1 = \Delta\alpha_j, \quad \delta_1 = \delta_0 + \Delta\delta_j, \quad dt_1 = \tilde{t}_j - t_1 \tag{32}$$

where the two angles of the sail are each changed within the following ranges.

$$-\frac{\pi}{2} < \alpha_1 < \frac{\pi}{2}, \quad -\frac{\pi}{2} < \delta_1 < \frac{\pi}{2} \tag{33}$$

Attitude control method

As a coupled model, station-keeping must be precisely controlled using the optimal sail angles, determined by the least-squares method. In this study, the target attitude is defined using quaternion composition, and attitude control is implemented through quaternion feedback, as shown in Eq. (15). In this case, the rotation around the z-axis is represented by a quaternion corresponding to the rotation angle α as follows:

$$q_z = \left[0, 0, \sin\frac{\alpha}{2}, \cos\frac{\alpha}{2}\right]^T \tag{34}$$

Next, the rotation around the y-axis is represented by a quaternion corresponding to the rotation angle δ as follows:

$$q_y = \left[0, \sin\frac{\delta}{2}, 0, \cos\frac{\delta}{2}\right]^T \tag{35}$$

The composition of the quaternions q_z and q_y is defined as follows:

$$q_{yz} = q_y \odot q_z \tag{36}$$

$$q_{yz} = \begin{bmatrix} q_{y,4}q_{z,1} + q_{y,1}q_{z,4} + q_{y,2}q_{z,3} - q_{y,3}q_{z,2} \\ q_{y,4}q_{z,2} - q_{y,1}q_{z,3} + q_{y,2}q_{z,4} + q_{y,3}q_{z,1} \\ q_{y,4}q_{z,3} + q_{y,1}q_{z,2} - q_{y,2}q_{z,1} + q_{y,3}q_{z,4} \\ q_{y,4}q_{z,4} - q_{y,1}q_{z,1} - q_{y,2}q_{z,2} - q_{y,3}q_{z,3} \end{bmatrix} \tag{37}$$

Summing up Eqs. (34),(35) and (36), each component of the synthetic quaternion is as follows:

$$q_{yz} = \left[\sin\frac{\delta}{2}\cos\frac{\alpha}{2}, \cos\frac{\delta}{2}\sin\frac{\alpha}{2}, \sin\frac{\delta}{2}\sin\frac{\alpha}{2}, \cos\frac{\delta}{2}\cos\frac{\alpha}{2}\right]^T \tag{38}$$

NUMERICAL SIMULATIONS

Ploblem settings

In the numerical simulation, a 9:2 resonant Near Rectilinear Halo Orbit(NRHO) near the L_2 point of the Earth-Moon system is adopted as the nominal orbit. The nominal orbit is shown in Fig. 5 and the initial orbit value and period of the nominal orbit are shown in Table 1. In particular, in this study, the IKAROS[21] values are adopted as references for the area and mass of the sail in numerical simulations.

To apply the station-keeping strategy, the three mission parameters needed to be defined: $\varepsilon_{\max}, dt_{\max}, dt_{\min}$. First, this study considers the following escape distances: $\varepsilon_{\max} = 1.0 \times 10^{-5}[-] \approx 3.844[\mathrm{km}]$. Next, set the minimum and maximum time between maneuvers: $dt_{\min} = 0.1[-] \approx 0.434[\mathrm{day}]$ and $dt_{\max} = 1.5[-] \approx 6.522[\mathrm{day}]$. Based on these mission parameters, this study conducted station-keeping operations near the nominal orbit for 30 orbital cycles.

For the control of the sail attitude (α, δ) during station-keeping, the time history of the sail obtained through numerical simulations is extracted and used as the target attitude angles. Attitude control is performed using quaternion feedback control. In this study, orbit control and attitude control are conducted independently; however, by implementing attitude control that considers disturbance torques acting on attitude motion due to the attitude changes required for orbit control, the framework of coupled motion is maintained.

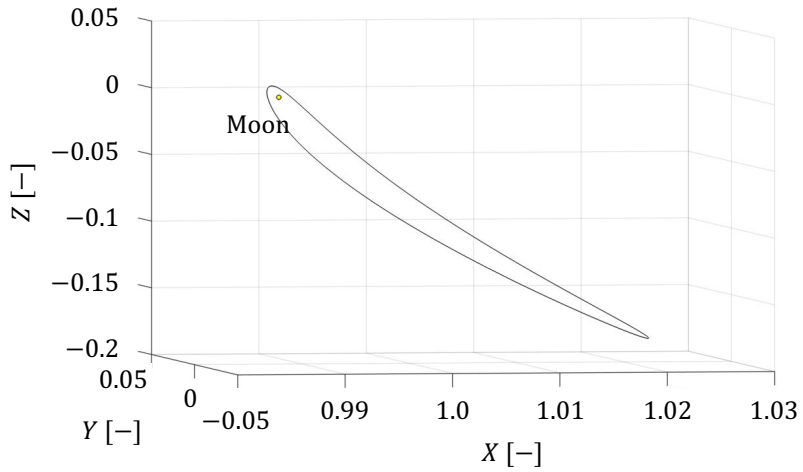

Figure 5: Nominal Orbit (9:2 resonant NRHO)

Table 1: Parameters of Nominal Orbit

Parameter	Value	Unit
x_0	1.0220261983	[-]
z_0	-0.182101410	[-]
$\dot{y}_0$	-0.103267465	[-]
T	1.511173498	[-]

Table 2: Optical Properties of Sail

Parameter	Value
C_a	0.053
C_d	0.882
C_s	0.065

Orbit control

Figures 6a and 6b show the time histories of the in-plane angle α and the out-of-plane angle δ, respectively, obtained using the least squares method. The in-plane angle α [deg] is changed within the range $\alpha \in [-22.86, 13.22]$ and the out-of-plane angle δ [deg] is changed within the range $\delta \in [-38.60, 23.38]$. By maintaining the optimal attitude for each optimal time dt_1, the sail returns to the nominal orbit, and the sail angle is maintained at the initial angle for a while.

Additionally, Fig. 7a shows the XY plane projection of the controlled trajectory, Fig. 7b presents the XZ plane projection, and Fig. 7c illustrates the XYZ spatial projection. These figures indicate that, during the 30 orbital cycles, the spacecraft trajectory remained close to the nominal orbit.

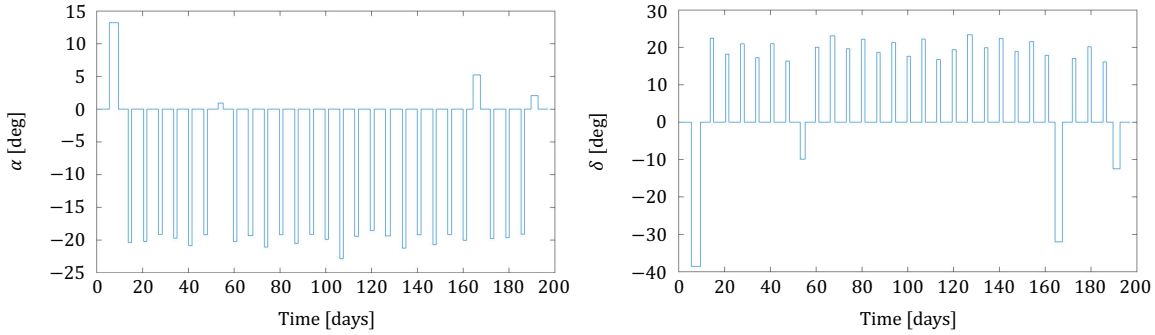

(a) In-Plane Angle α

(b) Out-of-Plane Angle δ

Figure 6: Time History of Sail Attitude

Attitude control

The solar sail spacecraft considered in this study has a structure where a large sail (membrane) is positioned $1.5[\mathrm{m}]$ away from the center of mass of a rectangular bus module. The physical characteristics of this structure and the moments of inertia for each axis are presented in Table 3. The proportional gain $(K_p = 10^6)$ and the derivative gain $(K_d = 20000)$ used in quaternion feedback for attitude control are configured to meet specific requirements. In this simulation, it is critically important to have quick response and high-precision attitude control. Consequently, the proportional gain is set high, while the derivative gain is carefully adjusted to prevent overshooting. It should be noted that modifying the control gains can further improve the precision of attitude control.

The optimized sail angles α and δ shown in Fig. 6a and Fig. 6b are converted to quaternions around each axis according to Eq. (38). From the composite quaternions using the converted q_z and q_y, the quaternions corresponding to α and δ are used as target values for tracking control. The time history of the quaternions in the control results is shown in Fig. 8. The black line represents the target quaternion based on the optimal α, δ, and the blue line represents the actual control output values.

For q_2, q_3, and q_4, the control output values are generally consistent with the target values, confirming sufficient tracking performance. On the other hand, for q_1, a slight oscillation remains when transitioning from the optimal angle to the initial angle, resulting in an error. The cause of this error can be attributed to the occurrence of overshoot due to the large control gain set to improve

Table 3: Physical Characteristics of the Solar Sail Spacecraft

Property	Value	Unit
Total mass (m)	310	kg
Bus dimensions ($L \times W \times H$)	$1.0 \times 1.0 \times 1.6$	m
Sail dimensions ($L \times W$)	$14 \times 14 \times 1.6$	m
Sail position	1.5	m
Moment of inertia about x-axis (J_x)	90.63	kg·m^2
Moment of inertia about y-axis (J_y)	61.63	kg·m^2
Moment of inertia about z-axis (J_z)	92.27	kg·m^2

responsiveness. Note that in this simulation, the control gain is set high for quick tracking to the target value, but such errors can be reduced by appropriate gain adjustment.

In numerical simulations based on the attitude dynamics, the GG torques from the Earth and Moon shown in Eq. (8) and the SRP torque shown in Eq. (12) are considered as disturbance torques. These disturbance torques are effectively attenuated by the quaternion feedback control according to the set control gains.

The results of converting controlled quaternions to sail angles α and δ are shown in Figs. 9a and 9b. From these figures, it is clear that the actual control results are in close correspondence with the target attitude angle, which indicates that the attitude control of the sail has been sufficiently achieved. This indicates that station keeping around the nominal orbit is feasible by the one-way coupled model control that takes into account the effect of the attitude motion on the orbit motion in the orbit-attitude coupled model.

Finally, Fig. 10 shows the actual attitude control torque generated by attitude control. The magnitude of the GG torque and SRP torque, which are disturbance torques in the attitude motion, is about 10^{-5} [Nm], respectively, while the control torque is output at about $10^{-4} \sim 10^{-3}$ [Nm]. This result indicates that the control torque sufficiently damps the disturbance torque and enables control to the target attitude.

CONCLUTION

This paper discusses the controllability of a solar sail orbiting on a 9:2 resonant orbit near point L in the Earth-Moon system. For the natural dynamics of the nominal orbit, the degree to which slight changes in the sail's attitude affect the subsequent orbit is calculated based on first-order flow, and a very simple station-keeping method is analyzed utilizing the Floquet mode. Using this method, it is confirmed that station-keeping is sufficiently useful, and furthermore, it is shown that it can be applied to periodic orbits other than resonant orbits.

In addition to station-keeping in orbit control, attitude control was also implemented to achieve optimal sail attitude. In attitude control, the GG torques from the Earth and Moon and SRP torque were considered as disturbance torques, but it was confirmed that the conventional method of quaternion feedback control was sufficient to control the attitude angle to the target attitude angle. Furthermore, we developed a framework for simultaneous control based on an orbit-attitude coupled model that not only controls orbit and attitude independently but also takes into account the effect of attitude motion on orbit motion.

REFERENCES

[1] J. Simo and C. R. McInnes,"Solar sail orbits at the Earth–Moon libration points," *Communications in Nonlinear Science and Numerical Simulation*,Vol. 14,No. 12,2009,pp. 4191–4196.

[2] D. Lujan and D. J. Scheeres,"FREQUENCY STRUCTURE OF THE NRHO FAMILY IN THE EARTH-MOON SYSTEM,"

[3] T. Kane and E. Marsh,"Attitude stability of a symmetric satellite at the equilibrium points in the restricted three-body problem," *Celestial mechanics*,Vol. 4,No. 1,1971,pp. 78–90, doi.org/10.1007/BF01230323.

[4] W. Robinson,"Attitude stability of a rigid body placed at an equilibrium point in the restricted problem of three bodies," *Celestial Mechanics and Dynamical Astronomy*,Vol. 10,No. 1,1947,pp. 17–333, 10.1007/BF01261876.

[5] A. Abad, M. Arribas, and A. Elipe,"On the attitude of a spacecraft near a Lagrangian point," *Bulletin of the Astronomical Institutes of Czechoslovakia*,Vol. 40,1989,pp. 302–307.

[6] E. Brucker and P. Gurfil,"Analysis of gravity-gradient-perturbed rotational dynamics at the collinear Lagrange points," *The Journal of the Astronautical Sciences*,Vol. 55,No. 3,2007,pp. 271–291, 10.1007/BF03256525.

[7] B. Wong, R. Patil, and A. Misra,"Attitude dynamics of rigid bodies in the vicinity of the Lagrangian points," *Journal of guidance, control, and dynamics*,Vol. 31,No. 1,2008,pp. 252–256, 10.2514/1.28844.

[8] D. Guzzetti and K. C. Howell,"Natural periodic orbit-attitude behaviors for rigid bodies in three-body periodic orbits," *Acta Astronautica*,Vol. 130,2017,pp. 97–113, 10.1016/j.actaastro.2016.06.025.

[9] A. J. Knutson, D. Guzzetti, K. C. Howell, and M. Lavagna,"Attitude responses in coupled orbit-attitude dynamical model in earth–moon lyapunov orbits," *Journal of Guidance, Control, and Dynamics*,Vol. 38,No. 7,2015,pp. 1264–1273, 10.2514/1.G000469.

[10] A. Colagrossi, V. Pesce, L. Bucci, F. Colombi, and M. Lavagna,"Guidance, navigation and control for 6DOF rendezvous in Cislunar multi-body environment," *Aerospace Science and Technology*,Vol. 114,2021,p. 106751, 10.1016/j.ast.2021.106751.

[11] A. Farrés and À. Jorba,"Periodic and quasi-periodic motions of a solar sail close to SL 1 in the Earth–Sun system," *Celestial Mechanics and Dynamical Astronomy*,Vol. 107,2010,pp. 233–253.

[12] S. Soldini,*Design and control of solar radiation pressure assisted missions in the sun-earth restricted three-body problem*. PhD thesis,University of Southampton,2016.

[13] C. Simó, G. Gómez, J. Llibre, R. Martinez, and J. Rodriguez,"On the optimal station keeping control of halo orbits," *Acta Astronautica*,Vol. 15,No. 6-7,1987,pp. 391–397.

[14] S. Kikuchi, K. C. Howell, Y. Tsuda, and J. Kawaguchi,"Orbit-attitude coupled motion around small bodies: Sun-synchronous orbits with Sun-tracking attitude motion," *Acta Astronautica*,Vol. 140,2017,pp. 34–48, 10.1016/j.actaastro.2017.07.043.

[15] S. Kikuchi, Y. Tsuda, M. Yoshikawa, and J. Kawaguchi,"Stability analysis of coupled Orbit–Attitude dynamics around asteroids using finite-time Lyapunov exponents," *Journal of Guidance, Control, and Dynamics*,Vol. 42,No. 6,2019,pp. 1289–1305.

[16] T. Chujo and Y. Takao,"Synodic resonant halo orbits of solar sails in restricted four-body problem," *Journal of Spacecraft and Rockets*,Vol. 59,No. 6,2022,pp. 2129–2147.

[17] T. Chujo,"Quasi-periodic orbits of small solar sails with time-varying attitude around Earth–Moon libration points," *Astrodynamics*,Vol. 8,No. 1,2024,pp. 161–174.

[18] A. Farrés and A. Jorba,"Station keeping of a solar sail around a halo orbit," *Acta Astronautica*,Vol. 94,No. 1,2014,pp. 527–539.

[19] G. Gómez, J. Llibre, R. Martínez, and C. Simó,*Dynamics and Mission Design Near Libration Points-Vol I: Fundamentals: The Case of Collinear Libration Points*,Vol. 2. World Scientific,2001.

[20] A. Farrés and A. Jorba,"On the station keeping of a solar sail in the elliptic Sun–Earth system," *Advances in Space Research*,Vol. 48,No. 11,2011,pp. 1785–1796.

[21] Y. Tsuda, O. Mori, R. Funase, H. Sawada, T. Yamamoto, T. Saiki, T. Endo, K. Yonekura, H. Hoshino, and J. Kawaguchi,"Achievement of IKAROS—Japanese deep space solar sail demonstration mission," *Acta Astronautica*,Vol. 82,No. 2,2013,pp. 183–188.

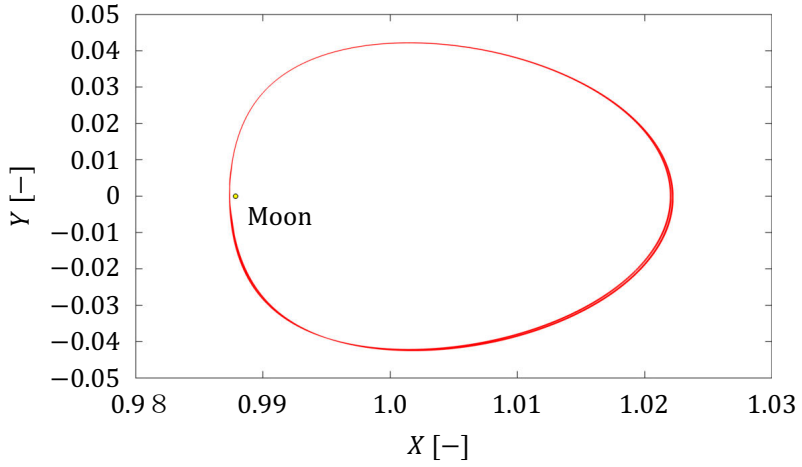

(a) XY Projection of Controlled Trajectory

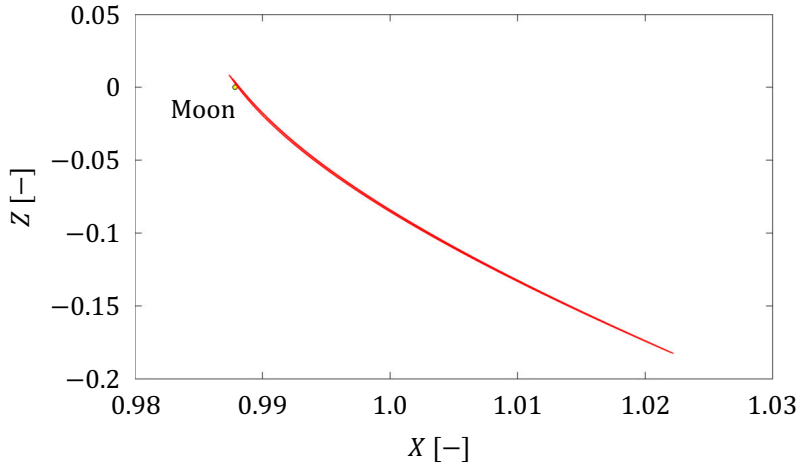

(b) XZ Projection of Controlled Trajectory

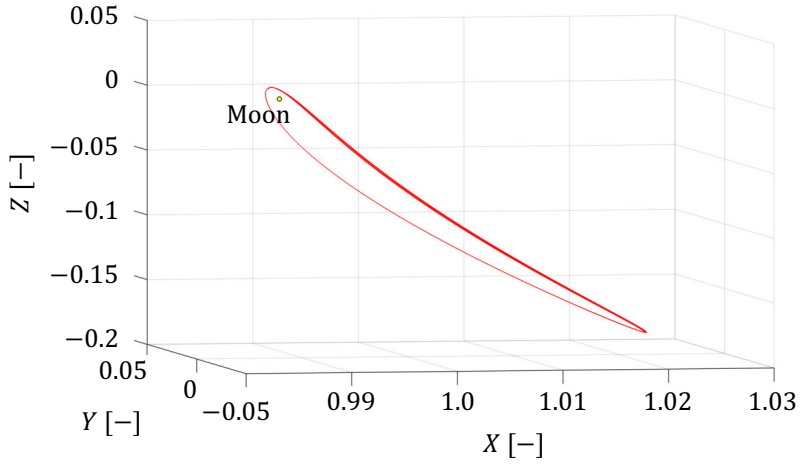

(c) XYZ Projection of Controlled Trajectory

Figure 7: Controlled Trajectory

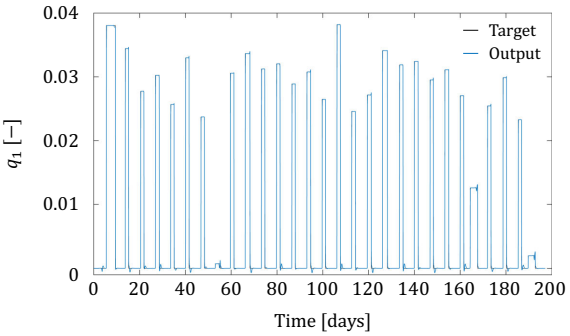

(a) Vector Part q_1

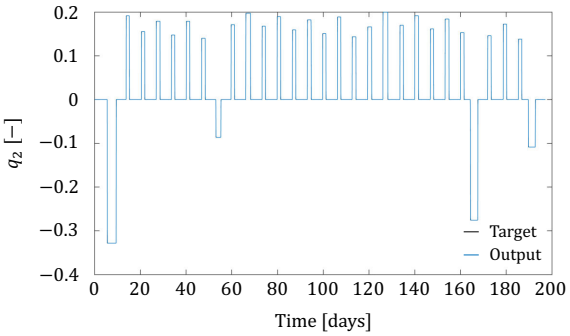

(b) Vector Part q_2

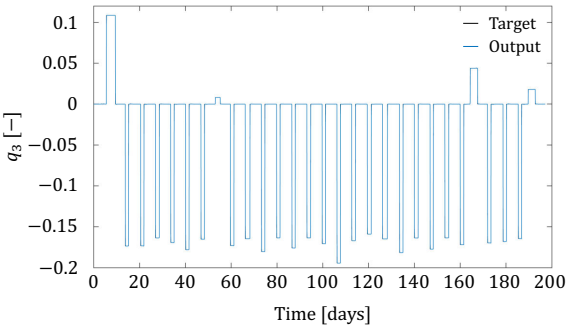

(c) Vector Part q_3

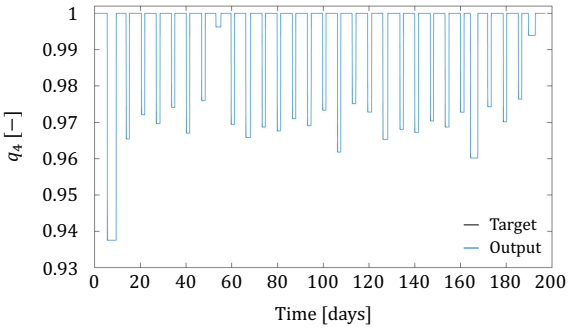

(d) Scalar Part q_4

Figure 8: Time History of Quaternion

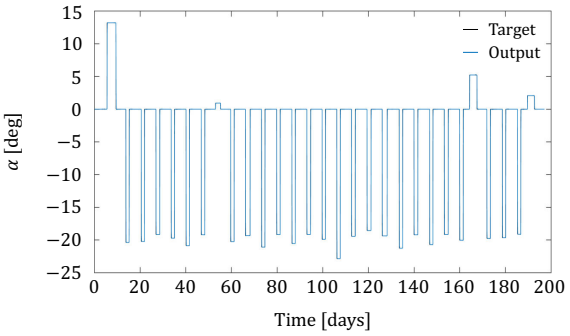

(a) In-Plane Angle α

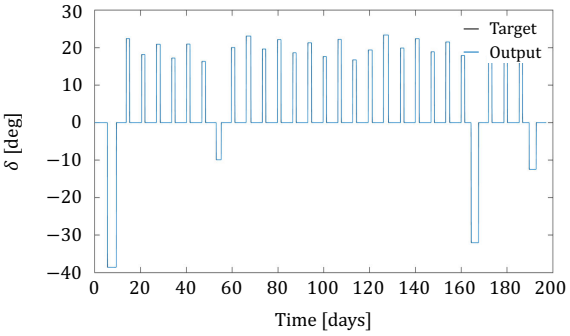

(b) Out-of-Plane Angle δ

Figure 9: Time History of Sail Angle

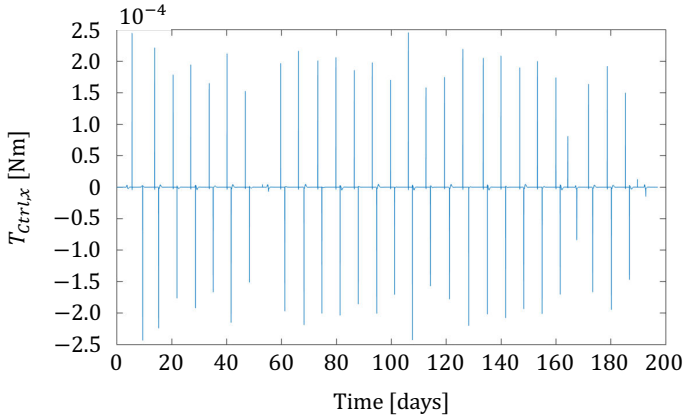

(a) Control Torque in x-Axis Direction

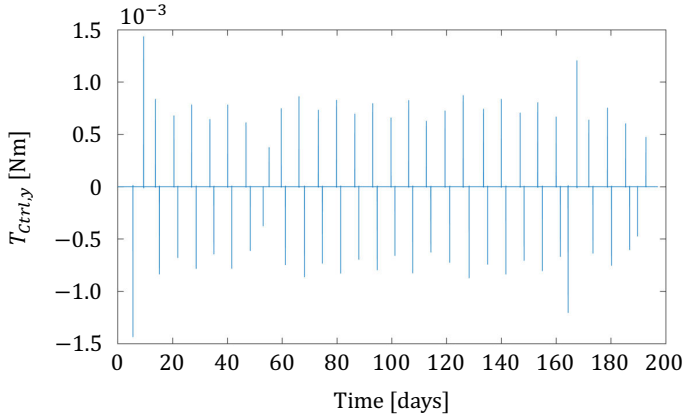

(b) Control Torque in y-Axis Direction

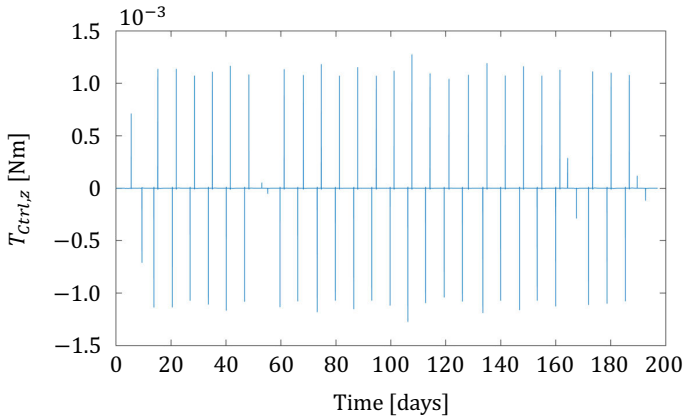

(c) Control Torque in z-Axis Direction

Figure 10: Time History of Controlled Torque in Each Axis Direction